

A prediction of the minke whale (*Balaenoptera acutorostrata*) middle-ear transfer function^{a)}

Andrew A. Tubelli^{b)} and Aleks Zosuls

Hearing Research Center and Department of Biomedical Engineering, Boston University,
44 Cummings Street, Boston, Massachusetts 02215

Darlene R. Ketten^{c)} and Maya Yamato

Biology Department, Woods Hole Oceanographic Institution, 266 Woods Hole Road, Woods Hole,
Massachusetts 02543

David C. Mountain

Hearing Research Center and Department of Biomedical Engineering, Boston University,
44 Cummings Street, Boston, Massachusetts 02215

(Received 13 January 2012; revised 13 July 2012; accepted 14 September 2012)

The lack of baleen whale (Cetacea Mysticeti) audiograms impedes the assessment of the impacts of anthropogenic noise on these animals. Estimates of audiograms, which are difficult to obtain behaviorally or electrophysiologically for baleen whales, can be made by simulating the audiogram as a series of components representing the outer, middle, and inner ear (Rosowski, 1991; Ruggero and Temchin, 2002). The middle-ear portion of the system can be represented by the middle-ear transfer function (METF), a measure of the transmission of acoustic energy from the external ear to the cochlea. An anatomically accurate finite element model of the minke whale (*Balaenoptera acutorostrata*) middle ear was developed to predict the METF for a mysticete species. The elastic moduli of the auditory ossicles were measured by using nanoindentation. Other mechanical properties were estimated from experimental stiffness measurements or from published values. The METF predicted a best frequency range between approximately 30 Hz and 7.5 kHz or between 100 Hz and 25 kHz depending on stimulation location. Parametric analysis found that the most sensitive parameters are the elastic moduli of the glove finger and joints and the Rayleigh damping stiffness coefficient β . The predicted hearing range matches well with the vocalization range.

© 2012 Acoustical Society of America. [<http://dx.doi.org/10.1121/1.4756950>]

PACS number(s): 43.64.Bt, 43.64.Ha, 43.64.Yp, 43.80.Lb [KG]

Pages: 3263–3272

I. INTRODUCTION

In order to assess the impact of anthropogenic noise on cetaceans, it is important to know their auditory thresholds as a function of frequency. Knowledge of hearing ranges for baleen whales, suborder Mysticeti, are particularly incomplete. There is some information on the spectra of sounds that these animals emit; for example, the minke whale emits sounds which range from 50 Hz to 9.4 kHz (Gedamke *et al.*, 2001). Vocalizations, however, do not provide enough information to evaluate hearing because many animals can hear beyond their vocalization frequencies (Ketten, 2002). Audiograms are available for numerous toothed whale (suborder Odontoceti) species. Mysticetes, however, are generally larger, more elusive, and not easily trainable, making it difficult to measure audiograms through behavioral or electrophysiological methods.

The ear can be thought of as a series of components which together determine the audiogram. An acoustic power-flow model was developed as a method of breaking down the auditory system into three components: one for the external ear, one for the middle ear, and one for the inner ear (Rosowski, 1991; Miller *et al.*, 2006). An audiogram captures the total effect from all three components. The middle ear is hypothesized to play a role in shaping the low to middle frequency regions of the audiogram (Ruggero and Temchin, 2002). The middle-ear transfer function (METF), in conjunction with cochlear properties and the sound pressure transformation occurring in the outer ear, can provide a more complete estimate of the audiogram.

Biologically realistic finite element (FE) models of the middle ear have been developed for terrestrial mammalian species (Wada *et al.*, 1990; Ladak and Funnell, 1996; Prendergast *et al.*, 1999; Koike *et al.*, 2002; Gan *et al.*, 2004; Elkhouri *et al.*, 2006; Homma *et al.*, 2009) and can be used to predict the METF. FE models have an advantage over other modeling approaches because they directly incorporate the geometry and material properties of the structures of interest.

Cetacean ears are similar in many characteristics to the ears of terrestrial mammals. There are, however, some notable anatomical differences. The outer ear of cetaceans is

^{a)}Portions of this work were presented in “Biomechanical analysis of hearing in whales using nanoindentation and the finite element method,” 11th International Workshop for the Mechanics of Hearing, Williamstown, MA, July, 2011.

^{b)}Author to whom correspondence should be addressed. Electronic mail: atubelli@bu.edu

^{c)}Also at: Department of Otolaryngology, Harvard Medical School, 243 Charles Street, Boston, Massachusetts 02114.

reduced and there is no external pinna (Ketten, 2000). The prototypical mammalian middle ear contains three ossicles, the malleus, incus, and stapes, housed inside a bony middle-ear cavity and connected with supporting ligaments and tendons. In cetaceans, the short process of the malleus is fused to the tympanic bone. In mysticetes, a “glove finger,” a hollow, everted fibrous structure, projects into the external auditory meatus of the outer ear. While the glove finger is homologous to the tympanic membrane typically seen in terrestrial mammalian ears (Fraser and Purves, 1954), its function is currently unknown. Additionally, mysticetes have enlarged middle-ear cavities with ossicles that are massive and loosely joined, a characteristic of a low-frequency ear (Ketten, 1994). The tympano-periotic bulla housing the middle ear in cetaceans is not a closed system as in terrestrial mammals, but rather open along its entire length on the medial side (Fleischer, 1978). The inner ear of cetaceans mainly differs in proportions, but is otherwise fundamentally the same as that of terrestrial mammals (Ketten, 2000).

The anatomical differences between aquatic and terrestrial mammals imply differences in sound transmission. In odontocetes, specialized perimandibular fat bodies that ultimately connect to the thin region of the tympanic bone are thought to play a role in sound transmission to the bulla (Norris, 1964; Cranford *et al.*, 2010). While sound reception mechanisms in mysticetes are unknown, recent work by Yamato *et al.* (2012) showed that there is fat body that contacts the thin region of the tympanic bone in mysticetes as well. A sound pathway to the cochlea for any cetacean species remains to be experimentally demonstrated.

The purpose of this study was to develop a detailed, anatomically accurate FE model of the middle ear of the minke whale (*Balaenoptera acutorostrata*) as a first step toward predicting the METF. The METF was estimated by measuring the frequency range of best transmission through the middle ear model given an applied pressure at two potential input locations: the tip of the glove finger and the thin region of the tympanic bone where the specialized fats abut.

II. FINITE ELEMENT MODEL

A. Anatomical reconstruction

A right minke ear complex (intact tympano-periotic bulla) was obtained from an animal which died through net entanglement. Post-mortem ear extraction was performed under a permit for scientific research on cetacean tissues issued to one of the authors (D.R.K.) and according to procedures described in Yamato *et al.* (2012). The ear was scanned using a Volume Zoom Spiral Computerized Tomography Scanner (Siemens AG, Munich) with ultra-high bone and mid soft tissue kernels. Images were reformatted at 0.1 mm isotropic voxels as well as $0.2 \times 0.2 \times 0.5$ mm voxels. The ear was scanned at the grosser resolution and fixed in formalin 6 days after death, and rescanned 33 days after initial fixation at the finer resolution. Both raw and DICOM images were archived.

The software program Amira (Mercury Computer Systems, Chelmsford, MA) was used to segment structures of interest in the DICOM image stack. The materials segmented in Amira included the malleus, incus, stapes, tympanic bone,

incudomalleolar joint, incudostapedial joint, annular ligament, and glove finger. The three-dimensional geometry was generated from the segmentation and artifacts were removed using Maya (Autodesk Inc., San Rafael, CA). The soft tissues in the reconstruction were within 15% of their respective volumes in the scans. The stapedius tendon, tensor tympani tendon, and posterior incudal ligament (collectively referred to here as the suspensory structures) were not reliably imaged in the scans because of their postmortem changes and inability to be distinguished from other soft tissue. These soft tissues were modeled instead in Maya as cylindrical (stapedius and tensor tympani tendons) or cuboidal (posterior incudal ligament) shaped. Ligament/tendon orientation and resting length from ossicle to respective attachment or recess into the periotic bone were determined during dissection. Their lengths were: stapedius tendon, 7.5 mm; tensor tympani tendon, 16.3 mm; posterior incudal ligament, 1.3 mm. The final reconstruction consisted of 4415 triangular elements and is shown in Fig. 1.

B. FE analysis

FE analysis of the middle ear model was performed using COMSOL Multiphysics (COMSOL Inc., Stockholm) to determine its frequency response. Modal analysis was also performed to determine its natural frequencies and the resulting deformations (i.e., its modes). The model was further meshed into 37 542 tetrahedral elements using COMSOL’s free mesher. The tympanic bone, glove finger, and suspensory structures were assigned a relatively coarse mesh size compared to the finer mesh size of the ossicles, joints, and annular ligament. The model was solved within the software.

C. Material properties

All components were modeled as homogeneous, isotropic, and linear for simplicity. Parametric analysis was performed to analyze the importance of uncertain parameters on the transfer function.

1. Bone elastic modulus

The elastic modulus of the minke whale ossicles was measured using nanoindentation with a TriboIndenter (Hysitron, Eden Prairie, MN). This equipment uses the Oliver-Pharr method to determine the reduced modulus of a sample via the unloading portion of a force-displacement curve (Oliver and Pharr, 1992). The reduced modulus E_r is related to the elastic modulus using the relation

$$\frac{1}{E_r} = \frac{(1 - \nu^2)}{E} + \frac{(1 - \nu_i^2)}{E_i} \quad (1)$$

where E and ν are the elastic modulus and Poisson’s ratio of the specimen, respectively, and E_i and ν_i are the elastic modulus and Poisson’s ratio of the indenter, respectively. A Berkovich tip was used for indentation, with E_i equal to 1140 GPa and ν_i equal to 0.07 (Oliver and Pharr, 1992). A value of 0.3 was used for ν (see Rho *et al.*, 1997). Indents were performed on a minke whale incus. The sample was mounted on a magnetic specimen disc with epoxy. After the epoxy

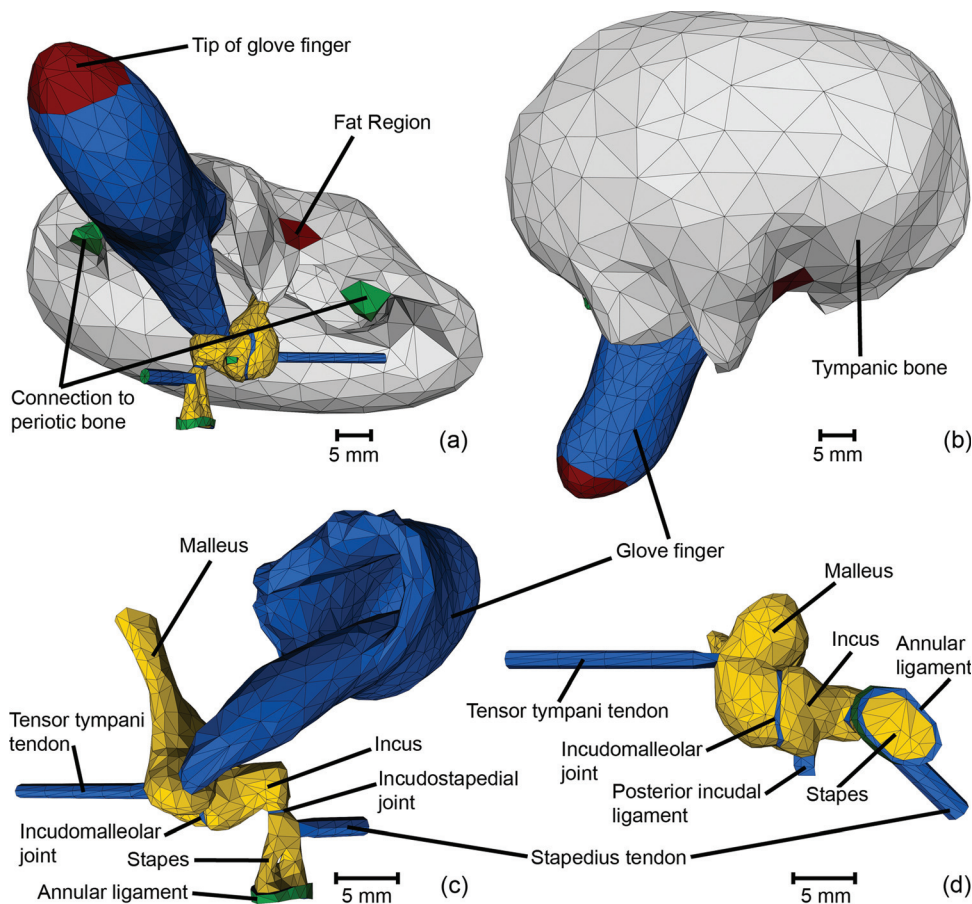


FIG. 1. Model geometry. (a) Lateral view, the labels show boundary conditions; (b) ventral view; (c) medial view minus tympanic bone; and (d) dorsal view minus tympanic bone and glove finger.

cured, the sample was cut level with a tile saw and polished using silicon carbide abrasive paper and lapping compounds of progressively finer grit (400, 600, 900, 1200, 3000). The interior region of the bone was indented. A load of 6 mN was applied at a rate of 100 μ N/s. The corresponding indentation depth for the incus was approximately 400 nm. Indents were calibrated on fused quartz. All bone was assumed to be isotropic and equal in elastic modulus value for FE analysis. The bones are likely inhomogeneous, although the effects of inhomogeneity were not explored in this study.

An average elastic modulus value of 29.7 ± 8.63 GPa was obtained for the incus. This was lower than the value of approximately 40 GPa obtained by Zioupos *et al.* (2005) for the fin whale (*Balaenoptera physalus*) tympanic bulla via nanoindentation, although similar to three-point bending tests on the fin whale tympanic bulla which gave an elastic modulus value of 31.1 GPa (Currey, 1978).

2. Soft tissue elastic modulus

The elastic moduli of the soft tissues of the cetacean ear are not currently known. The glove finger elastic modulus was based on values used for the pars flaccida in other middle-ear FE studies since the glove finger is most similar in structure to the pars flaccida (Fraser and Purves, 1954). The base value (defined as the default model value used before parametric analysis) was the average of the values used by Homma *et al.* (2009) and Elkhouri *et al.* (2006): 7 MPa and 20 MPa, respectively. These two numbers served as the low and high values for parametric analysis.

Measurements of middle ear mechanical stiffness were used to determine the elastic moduli of the remaining soft tissues. The middle-ear reverse stiffness of two minke ears was measured using the same equipment and methods as described in Miller *et al.* (2006). Reverse stiffness is defined as the force required to drive the stapes footplate for a given displacement. Reverse stiffness is used since the stapes footplate is known to be the termination of the middle ear, whereas the location of the input to the middle ear in cetaceans is less certain.

Two right minke whale tympano-periotic bullae were extracted from the heads of two different specimens and immersed in phosphate-buffered normal saline solution. The cause of death for Specimen 1 is unknown; Specimen 2 was found entangled in fishing gear. The ears were refrigerated at 4 °C rather than frozen to maintain preservation since the formation of ice crystals during the freezing process can damage tissue. Measurements were made three days after animal death in both specimens.

The cochlear vestibule was carefully opened with a dental drill to expose the stapes footplate. The ear was then mounted on a force probe apparatus as described in Miller *et al.* (2006). Stiffness was measured as the force required to displace the stapes in and out of the annular ligament. Piston-like motion was assumed. To keep the measurement physiologically relevant, the displacement of the stapes was kept as small as possible at less than 3 μ m. The incus joints were damaged during extraction of one minke ear, allowing measurement of the intact ossicular chain on only one ear. Disarticulated middle ear stiffness is defined here as the stiffness of

the stapes supported only by the annular ligament and stapedius muscle. Disarticulated middle ear stiffness was measured on both ears. Both intact and disarticulated reverse stiffness were measured in three trials for Specimen 1 and disarticulated reverse stiffness was measured in two trials for Specimen 2.

FE models of both intact and disarticulated ears were developed to compare stiffness results. Pressure was applied to the footplate of the stapes; all other boundary conditions and material properties were the same as described above. The disarticulated model only included the stapes, annular ligament, and stapedius tendon geometries. Stiffness was calculated as the input pressure times the area of footplate displacement divided by the displacement at the center of the stapes footplate. The disarticulated middle ear model was used to find a combination of annular ligament and stapedius tendon elastic moduli which produced a comparable stiffness to experimental results. The remaining soft tissues were assumed to have a model stiffness equal to that of the stapedius tendon. The intact middle ear model was used to verify these choices by comparing model and experimental intact stiffness.

Figure 2 shows a typical example of the results obtained from reverse stiffness measurement. Figures 2(a) and 2(b) show the magnitude and phase, respectively. Figure 2(c) plots the total harmonic distortion (THD), the ratio of the root mean square of the signal harmonic power to the root mean square power of the total signal. THD is large when the probe is in partial contact due to tapping of the probe on the footplate. THD decreases and asymptotes as the probe comes into full contact with the stapes footplate. Stiffness was determined as the point on the magnitude plot where, simultaneously, the THD curves for an advancing and retracting probe converged and the phase was stable. This point corresponds to full contact with the stapes while the stapes is still at rest position. Since stiffness changes very

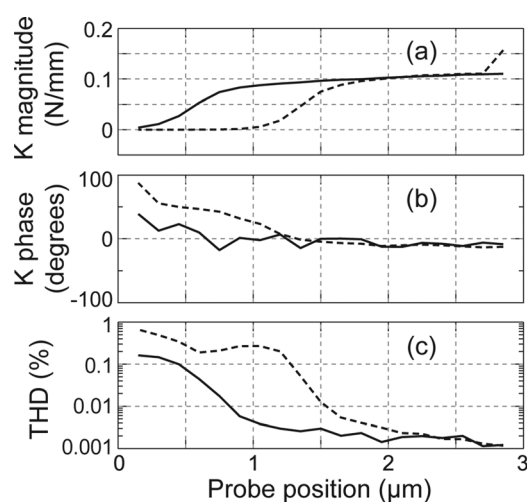


FIG. 2. A typical middle-ear reverse stiffness (K) measurement. Solid lines represent advancement of the probe toward the stapes footplate and dotted lines represent retraction of the probe from the stapes footplate. (a) Magnitude, (b) phase, and (c) THD are plotted as a function of probe position. This plot shows the results from the first trial for an intact ear in Specimen 1 (stiffness = 0.104 N/mm).

TABLE I. Experimental and model results for the reverse middle-ear stiffness of the intact and disarticulated ear. Intact data for minke whale Specimen 2 is unavailable. Only two trials for disarticulated stiffness for Specimen 2 were performed.

		Stiffness (N/mm)		
		Experiment		
		Specimen 1	Specimen 2	Model
Intact	Trial 1	104		
	Trial 2	79	–	94.89
	Trial 3	83.4		
Disarticulated	Trial 1	8.5	14	
	Trial 2	8.2	13.5	11.71
	Trial 3	8.3	–	

little after the probe gains full contact with the stapes footplate, measurements were assumed to be in the linear range.

The reverse stiffness values obtained for each trial for both minke specimens are listed in Table I. Model stiffness results are listed alongside the experimental values. The average stiffness on Specimen 1 when disarticulated was 8.33 N/mm. Specimen 2 had an average disarticulated reverse stiffness of 13.75 N/mm. The average between the two species was 11.04 N/mm. Model elastic moduli values of 9×10^5 Pa and 1×10^7 Pa for the annular ligament and stapedius tendon, respectively, produced a model stiffness that was within 1% of the average disarticulated stiffness. Intact model stiffness is within 7% of the average intact reverse stiffness for Specimen 1 (88.8 N/mm).

Elastic moduli were varied by one order of magnitude lower and higher for parametric analysis with the exception of the high value for the incudomalleolar joint. The incudomalleolar joint is typically assumed to be rigid in other middle-ear FE models. Evidence of differential motion between the malleus and incus (Willi *et al.*, 2002) suggests that the joint is more compliant; therefore, the high value of elastic modulus used for parametric analysis of the incudomalleolar joint was that of the surrounding bone to determine whether a rigid connection can be reasonably assumed.

3. Density

The density of all three ossicles has been previously measured by Nummela *et al.* (1999) for six mysticete species (*Balaenoptera borealis*, *Balaenoptera physalus*, *Balaenoptera musculus*, *Megaptera novaeangliae*, *Eubalaena glacialis*, and *Balaena mysticetus*). Since the values do not change significantly between any of the species, an average value for each ossicle was used for each respective ossicle in the minke whale model. The tympanic bone was assumed to have the same density as the malleus. These values of density were within 8% of the density calculated from the mass of available minke whale ossicles and the volume of the reconstructed ossicles.

There are no values available for the density of cetacean soft tissues of the middle ear. The values of soft tissue densities were instead taken from human values, which are assumed to have similar properties as other mammalian soft

TABLE II. Elastic modulus and density of all model components.

Component	Elastic modulus (N/m ²)	Density (kg/m ³)
Tympanic bone	2.97×10^{10}	2.35×10^3 ^a
Malleus	2.97×10^{10}	2.35×10^3 ^a
Incus	2.97×10^{10}	2.39×10^3 ^a
Stapes	2.97×10^{10}	2.32×10^3 ^a
Glove finger	1.35×10^7	1.20×10^3 ^b
Annular ligament	9.00×10^5	1.20×10^3 ^c
Tensor tympani tendon	1.00×10^7	1.20×10^3 ^c
Stapedius tendon	1.00×10^7	1.20×10^3 ^c
Posterior incudal ligament	1.00×10^7	1.20×10^3 ^c
Incudostapedial joint	1.00×10^7	1.20×10^3 ^c
Incudomalleolar joint	1.00×10^7	1.20×10^3 ^c

^aNummela *et al.* (1999).^bWada *et al.* (1990).^cHomma *et al.* (2009).

tissues. The value of density for the glove finger was that of the tympanic membrane measured by Wada *et al.* (1990). The values of all other soft tissues that were used for the minke whale middle-ear model were taken from Homma *et al.* (2009). All density values of the model components are listed in Table II.

4. Poisson's ratio

The value of Poisson's ratio used for bone was 0.3, a common value seen in middle-ear FE models. The soft tissues were modeled as nearly incompressible with Poisson's ratio set to 0.45.

5. Damping

The effect of the cochlear load was modeled by using damping in the form of a pressure on the stapes footplate. The pressure was calculated as the cochlear damping constant times velocity of the stapes footplate divided by footplate area. Of the mammals with available cochlear input impedance measurements, the minke whale has a cross-sectional area that is closest to human. A cochlear damping constant of 0.217 N s/m was calculated assuming a constant cochlear input impedance of 21.1 GΩ and stapes footplate area measured by Aibara *et al.* (2001). The effect of cochlear damping on the model was determined with parametric analysis, using 0.059 N s/m as the low value calculated from Puria (2003), and 0.891 N s/m as the high value used by Koike *et al.* (2002).

Rayleigh damping, an estimate of damping in complex vibrating systems, was also applied to the entire middle-ear structure. The equation to calculate the system damping matrix $[C]$ is given by

$$[C] = \alpha[M] + \beta[K] \quad (2)$$

where $[M]$ and $[K]$ represent the mass and stiffness matrices of the system, respectively, and α and β are damping coefficients. The values used were $\alpha = 0 \text{ s}^{-1}$ and $\beta = 1 \times 10^5 \text{ s}$, which were on the order used in other publications (e.g., Gan *et al.*, 2004; Koike *et al.*, 2002; Prendergast *et al.*, 1999).

While α did not change across most sources, β was variable. The effects of decreasing damping parameter β by one and two orders of magnitude were determined using parametric analysis.

D. Boundary conditions

The fluid of the cochlea is driven mechanically by means of the stapes footplate pushing in and out of the oval window. In order for this to occur, there must be differential motion between the periotic bone and the stapes, or effectively the entire ossicular chain. The boundary conditions were chosen to reflect this. The edges of the soft tissues located distally from the ossicles were fixed. The edges of the tympanic bone at the two bony processes where it connects to the periotic bone were also given a fixed boundary condition.

The magnitude of pressure is arbitrary since the model is linear. The value was nevertheless chosen so that stapes footplate displacements for the model were on the same order as those from experiments described in Sec. IIC 2. Pressure was applied normal to the surface at two potential sound input locations, each with their own assumptions regarding how sound enters the middle ear. The "glove finger" model (GFM) is stimulated by applying a normal force to the elements that make up the tip of the glove finger, an area of about 160 mm². This model assumes that the glove finger has retained its function as a tympanic membrane in the minke whale. The "tympanic bone" model (TBM) is stimulated by applying a normal force to the elements in the thin region of the tympanic bone, an area of 41.2 mm², where the specialized fats of the mysticetes abut. The TBM assumes that mysticete tympanic bones possess a sound input mechanism somewhat similar to that of odontocetes. Both areas of input can be seen in Fig. 1. The effects of a larger and smaller area of each location on the METF were also considered. The glove finger region was varied from 79.6 mm² to 280 mm². The tympanic bone region was varied from 6.6 mm² to 77.8 mm².

E. Transfer function

The transfer function was computed as the velocity at the center of the stapes footplate in the direction perpendicular to the footplate divided by the input pressure and expressed in units of nm/Pa s.

III. RESULTS

A. METF

The METFs obtained for the GFM and TBM are shown in Fig. 3. The model is more sensitive to stimulation at the glove finger than at the tympanic bone for frequencies below 4 kHz. At higher frequencies, the GFM METF attenuates sharply and the TBM METF has a greater magnitude.

The GFM METF shows many strong resonances at the middle frequencies (0.1–5 kHz) as determined by modal analysis. Pronounced peaks in the transfer function at around 180 Hz, 250 Hz, 460 Hz, and 750 Hz correspond to modes dominated by the glove finger. The mode at 250 Hz is characterized by stretching of the glove finger principally in the posterolateral direction, i.e., along its length; all other modes

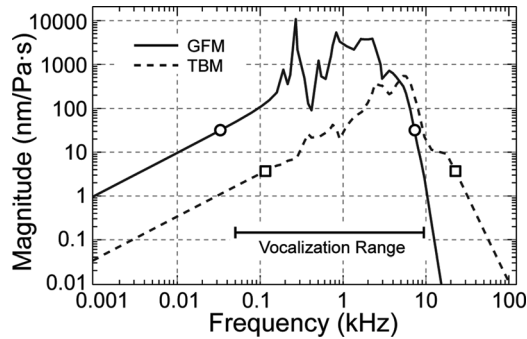


FIG. 3. Middle-ear transfer functions for the GFM and TBM. Circles indicate the -40 dB bandwidth for the GFM, squares indicate the -40 dB bandwidth for the TBM. Vocalization range is based on findings from *Gedamke et al. (2001)*.

also involve stretching of the glove finger in various directions, some component of which is along its length. Resonances in the tympanic bone dominate two modes: one around 330 Hz and one around 800 Hz. The mode shapes are characterized by rocking of the whole tympanic bone about the two processes connecting to the petiotic bone. These two modes correspond to peaks in the METF for the TBM.

B. Parametric analysis

Parametric analysis was performed only on those parameters that were considered uncertain. Physiological ranges were used for each parameter when known, as described in methods.

The GFM is sensitive to the elastic modulus of the glove finger, shown in Fig. 4(a). An increase in the glove finger elastic modulus shifts the mid- and high-frequency peaks to higher frequencies. The high-frequency slope is subsequently shifted, slightly increasing bandwidth. A decrease in glove finger elastic modulus has the opposite effect. In either case, the low-frequency slope remains unaffected. The elastic

modulus of the glove finger did not significantly affect the TBM METF when varied an order of magnitude greater or less than the base value.

The annular ligament affects the METF primarily in magnitude. The response of the TBM and GFM METFs to change in the annular ligament elastic modulus are quantitatively similar. A parameter value one order of magnitude greater shifts the METF lower in magnitude by about 6 dB across low and middle frequencies, less at frequencies beyond 5 kHz. When the annular ligament elastic modulus is reduced by one order of magnitude, the GFM METF shifts higher by approximately 1 dB, less at frequencies beyond 3.5 kHz.

Changes in the incudomalleolar joint elastic modulus have the greatest effect at high frequencies, starting around 4 kHz. Since the GFM METF drops off sharply and sooner than the TBM METF, a greater effect is seen for the TBM, as shown in Fig. 4(b). A lower value produces a steeper high-frequency slope and vice versa. The METF decreases up to 20 dB at 100 kHz for a decreased elastic modulus and increases 30 dB for an increased elastic modulus (i.e., when the elastic modulus was equal to that of bone). Low and middle frequencies showed only slight change, shifting in magnitude by 3 dB or less.

The response of the METF to changes in the incudostapedial joint elastic modulus is qualitatively similar to the response observed when changing the incudomalleolar joint elastic modulus. The METF decreases by approximately 20 dB at 100 kHz for a decreased elastic modulus and increases up to 18 dB for an increased elastic modulus. The low and middle frequencies only shifted by 3 dB or less.

The elastic moduli of the suspensory structures do not significantly affect the METF for either model when varied an order of magnitude greater or less than the base value. Changes in the cochlear damping coefficient within the range of physiological values also produce a negligible effect on the METF for either model.

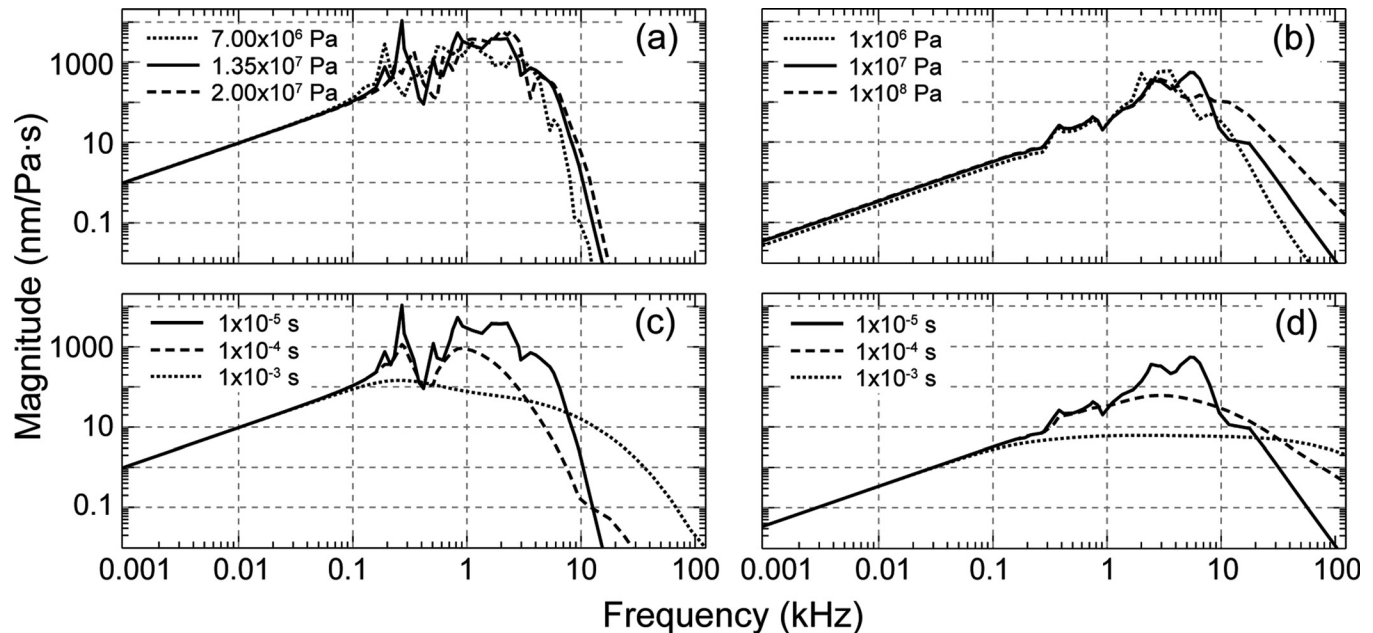


FIG. 4. METF parametric analysis. The parameters that are shown are (a) elastic modulus of the glove finger, GFM, (b) elastic modulus of the incudomalleolar joint, TBM, (c) Rayleigh damping stiffness coefficient β , GFM, and (d) β , TBM.

Changing β affects the shape of the METF at frequencies beyond the low-frequency slope for both the GFM, shown in Fig. 4(c), and TBM, shown in Fig. 4(d). Increasing β reduces the slope of the high frequency roll-off thus extending the bandwidth. The magnitude also decreases while simultaneously producing a smoother METF with fewer peaks and troughs.

The size of the input area while maintaining a constant pressure, i.e., changing the force, also affects the transfer function magnitude. The TBM shows an approximate 1:1 proportional change in METF magnitude to the change in input area. Increasing the GFM input area to 280 mm² (an increase of 75%) shifted the METF higher by 3 dB up to its high-frequency drop-off at 10 kHz with no significant change in bandwidth. Decreasing the GFM input area to 79.6 mm² (a decrease of 50%) shifted the METF lower by 5 dB up to its high-frequency drop-off.

IV. DISCUSSION

The range of best frequencies predicted by the model was chosen based on the -40 dB bandwidth in order to provide a range of frequencies fit for comparison to the vocalization frequency range. MATLAB (MathWorks, Natick, MA) was used to smooth the METF curve (smooth function, rlowess filter, span of 0.2) in order to calculate the maximum value to serve as a reference to the -40 dB bandwidth. The range of best frequencies for the GFM is approximately 30 Hz to 7.5 kHz. The TBM has a best frequency range of approximately 100 Hz to 25 kHz. In comparison, the vocalization frequencies of the minke whale measured by [Gedamke et al. \(2001\)](#) were between 50 Hz and 9.4 kHz. Nearly all of these vocalization frequencies fall within the -40 dB bandwidth of the GFM METF; additionally, the METF for the GFM has a higher magnitude at most of these frequencies than does that of the TBM.

The low-frequency slope of the METF predicted by the minke whale middle-ear model is 20 dB/decade. Cetacean audiograms typically have a low-frequency slope of 40 dB/decade ([Wartzok and Ketten, 1999](#)). If the middle ear is modeled as a simple mass-spring system, a low-frequency slope of 20 dB/decade is expected for a system dominated by a single spring component. In the case of the model, the spring is represented by the middle-ear stiffness, comprised primarily of the stiffness of the annular ligament and the bony connection between the malleus and the tympanic bone for cetaceans ([Fleischer, 1978](#); [Miller et al., 2006](#)). The extra 20 dB/decade is likely to be caused in part by the loss of pressure difference at low frequencies across the sensing surface as a result of having an open auditory bulla. Due to its medial opening, the tympano-periotic bulla may act as a pressure gradient microphone (as described by [Beranek, 1954](#)), in which the pressure difference across the glove finger or tympanic bone would be equal to the pressure difference between the input location and the open side of the bulla.

The effect of the helicotrema, an opening at the apex of the cochlea between the scala vestibuli and the scala tympani, is also expected to increase the low-frequency slope. At low frequencies, the helicotrema functions as an acoustic shunt.

The cochlear input impedance is strongly affected at these frequencies. This, in turn, affects the low-frequency cut-off, which is inversely proportional to the square of the radius of the helicotrema ([Dallos, 1970](#)). The dimensions of the helicotrema in the minke whale are unknown.

The high frequency limit of the audiogram is more likely to be governed by the upper frequency limit determined by the stiffness and dimensions of the basilar membrane ([von Békésy, 1960](#)). Even if the METF predicts good high-frequency hearing in these animals, these frequencies will not be detected by the animal if there is no corresponding spot to receive such signals along the length of the cochlea. In order to further estimate an audiogram, more information about the mechanics of the basilar membrane must be known.

The response of the GFM to changes in the glove finger elastic modulus is similar to that of changing the tympanic membrane elastic modulus in humans. According to [Gan et al. \(2004\)](#), reducing the elastic modulus of the tympanic membrane by one order of magnitude caused the response peak to shift lower in frequency, and the high frequency response was reduced. The opposite is true for increasing the tympanic membrane elastic modulus. The GFM model reacted in a similar way at frequencies greater than 100 Hz. The results from [Gan et al. \(2004\)](#) only go as low as 200 Hz, so lower frequencies cannot be compared. The lack of change in response at lower frequencies is likely an effect of the structure of the glove finger. Unlike the conically shaped tympanic membrane supported around its circumference, the glove finger consists of a tube suspended around the middle of its length with a ligament-like connection to the malleus.

Decreases in the joint elastic moduli shifted the transfer function lower in magnitude and decreased the bandwidth. This change is likely caused by the decrease in efficiency when the bones are decoupled as a result from increasing the compliance of the connections. The opposite is true of the annular ligament: increased compliance improves efficiency, although slightly. This is likely because the main source of stiffness is the bony connection between the malleus and tympanic bone. Also, the high-frequency response is affected when the elastic moduli of the joints are changed. Changing the incudomalleolar joint stiffness by one order of magnitude can change the high-frequency response by as much as 30 dB. These results suggest that it may not necessarily be a reasonable assumption to model the incudomalleolar joint as rigid.

Cochlear damping had an insignificant effect on the transfer function. [Gan et al. \(2004\)](#) showed that by removing the cochlear load, the resulting stapes displacements were higher at frequencies greater than 1 kHz. Rather than removing the cochlear damping, we varied the cochlear damping constant between 0.059 Ns/m and 0.891 Ns/m. While the results are in agreement that frequencies above 1 kHz are affected, the change was not as large and the results from those changes were not significant.

The linear effect of changing the input area on the TBM METF was expected since the additional input area is approximately planar with the original input area. The glove finger did not respond with a 1:1 ratio of parameter change to METF magnitude change. This is likely because the tip of the glove finger is not planar. Additional input area means force

must be applied along the length of the glove finger until the force is essentially perpendicular to the normal vector of the tip, an inefficient direction for propagation of motion.

To the limited extent that our interpretation of the transfer function can predict a sound transmission pathway into the middle ear, it appears that each input gives a distinct response: the glove finger is a more efficient pathway for lower frequencies and the thin region of the tympanic bone is a more efficient pathway for higher frequencies. Even with comparable force at each location (constant pressure and areas at the glove finger and tympanic bone input locations of 77.8 mm² and 79.6 mm², respectively), the glove finger provides a greater stapes velocity at lower frequencies. Since the GFM METF also matches up well with vocalization frequencies, if the properties of the middle ear are as predicted, the glove finger is more favorable as the primary input location of sound to the middle ear. If the thin region of the tympanic bulla were functional for sound reception as well, it would likely be a secondary input better suited for higher frequencies.

We can use the model results to compare stapes motion at threshold of the minke whale middle-ear model to experimental data from terrestrial mammals. Assuming the glove finger is the input to the model, the peak of the METF occurs around 2 kHz when smoothed (MATLAB smooth function, rlowess filter, span of 0.2). The hearing threshold in water for the minke whale is assumed to be similar to odontocete thresholds, about 70 dB re 1 μPa at 2 kHz for the bottlenose dolphin and killer whale (Johnson, 1968; Szymanski *et al.*, 1999). Alternatively, it is likely that the minke whale threshold is near the ambient noise level. At 2 kHz for a smooth sea, no wind, the ambient spectral density is about 45 dB re 1 μPa²/Hz (Kibblewhite and Jones, 1976). To convert to a threshold pressure we must have an estimate of the critical bandwidth or critical ratio. These values are not available for the minke whale so the critical ratio (20 dB at 2 kHz) for the beluga whale was used (Johnson *et al.*, 1989). This leads to a predicted threshold of 65 dB re 1 μPa, a value similar to the measured odontocete thresholds. Using 70 dB re 1 μPa for the minke threshold leads to a calculated stapes velocity of 10 nm/s, which is similar to the velocity calculated at threshold for other mammals (Table III).

There are some important caveats in the model. First, the model uses a mechanical stimulus rather than an acoustic one. While the acoustic stimulus can be modeled as a mechanical input, the properties of the tissues surrounding the tympano-periotic complex must be known to approximate the correct mechanical counterpart.

Second, the boundary conditions of the model are simplified. For example, the external auditory meatus in mysticetes is not air-filled and unobstructed as in terrestrial mammals: mysticetes have a plug composed of layered cholesterol and keratinized epithelium between the glove finger and the external auditory meatus (Purves, 1955). It remains to be determined whether this plug has any impact on hearing, but its properties should be reflected in the pressure applied to the glove finger. Also, the glove finger is almost entirely surrounded by bone along its length except for its ventral anterior surface (Yamato *et al.*, 2012). These conditions were not explored in the present model.

TABLE III. Stapes motion calculated for four terrestrial species compared to predicted motion for the minke whale middle-ear model. Footplate areas were used to convert units for gerbil, chinchilla, and cat; footplate areas for human and minke whale are listed for comparison. The calculated velocities are those at threshold and at the best frequency of the METF for each species.

	METF magnitude peak	Footplate area (mm ²)	Threshold (dB)	Stapes velocity (nm/s)
Gerbil	0.2 mm ³ /Pa s ^a	0.62 ^b	2.68 re 20 μPa ^c	8.79
Chinchilla	0.5 mm ³ /Pa s ^a	2.0 ^d	5 re 20 μPa ^c	8.9
Cat	0.2 mm ³ /Pa s ^a	1.26 ^f	0 re 20 μPa ^g	3.18
Human	0.3 mm ³ /Pa s ^h	3.2 ⁱ	-6.5 re 20 μPa ^j	2.84
Minke whale	3.2 × 10 ⁻³ mm ³ /Pa s	11.8	70 re 1 μPa ^{k,l}	10

^aRosowski (1994).

^bLay (1972).

^cRyan (1976).

^dRuggero *et al.* (1990).

^eHeffner and Heffner (1991).

^fGuinan and Peake (1967).

^gHeffner and Heffner (1985).

^hAibara *et al.* (2001).

ⁱWever and Lawrence (1954).

^jISO 389-7 (1996).

^kJohnson (1968).

^lSzymanski *et al.* (1999).

The TBM model assumes that mysticete tympanic bones possess a sound input system somewhat similar to that of odontocetes. Indeed, the ear fats described in Yamato *et al.* (2012) come into contact with the region of the tympanic bone that was perturbed in our model. However, the ear fats also insert into the tympano-periotic complex and contact the ossicles in the minke whale. This has not been described for odontocetes and was not reflected in our model.

Finally, our analysis relies on the hypothesis that the audiogram can be assembled from components: one for the external ear, one for the middle ear, and one for the cochlea (Rosowski, 1991; Ruggero and Temchin, 2002). Assuming that the middle ear component is defined by the transfer function, the model results will give some indication of the range of frequencies that can be heard by the whale. Theoretically, the METF is good for estimating the low to middle frequency regions of the audiogram. The cochlear input impedance may also be an important factor in determining the low-frequency limit of the audiogram (Ruggero and Temchin, 2002). The model showed very little sensitivity to changes in the cochlear input impedance, although this parameter was simplified for the model.

The results of the model indicate that many anthropogenic noise sources operate at similar frequencies to those heard by the minke whale. Shipping traffic is a primary source of noise in the ocean between 50 and 500 Hz (Urlick, 1983). Noise generated by seismic airgun arrays also has an effect at lower frequencies up to 300 Hz with source levels up to 255 dB re 1 μPa. At higher frequencies, military sonar (1–10 kHz) can produce source levels greater than 210 dB re 1 μPa (Nowacek *et al.*, 2007).

V. CONCLUSIONS

Audiograms of mysticetes are needed to understand how these species may be affected by anthropogenic noise.

The METF of the minke whale can be used as part of a first attempt to estimate the frequency range that can be heard for this species. In this study, an anatomically accurate model of the minke whale middle ear was created, incorporating both bone and soft tissues. The resulting METF displays a best frequency range for the minke whale of between approximately 30 Hz and 7.5 kHz when stimulated at the glove finger, and between approximately 100 Hz and 25 kHz when stimulated at the thin region of the tympanic bone. Parametric analysis was conducted to determine which material properties, most of which are unknown for mysticete tissues, have the greatest effect on the METF. The parameters with the greatest influence on the METF and the frequencies that are most sensitive are glove finger elastic modulus (>100 Hz), annular ligament elastic modulus (<3.5 kHz), incudomalleolar joint elastic modulus (>4 kHz), incudostapedial joint elastic modulus (>4 kHz), and β (>100 Hz). Future research involving material property measurements should be combined with the results of this study in order to obtain a more refined model assessment of whale hearing.

ACKNOWLEDGMENTS

The authors wish to thank the Office of Naval Research for funding this study. Additionally, the authors thank the reviewers, Dr. John Rosowski and two anonymous editors, for contributing their time and expertise to strengthening the quality of the paper. The International Fund for Animal Welfare's Marine Mammal Rescue and Research Group generously provided the minke whale specimens used in this research. The authors would also like to thank Julie Arruda and Scott Cramer at the Woods Hole Oceanographic Institution Computerized Imaging Facility for help in scanning and preparing specimens.

Aibara, R., Welsh, J. T., Puria, S., and Goode, R. L. (2001). "Human middle-ear sound transfer function and cochlear input impedance," *Hear. Res.* **152**, 100–109.

Beranek, L. L. (1954). *Acoustics* (McGraw-Hill, New York), pp. 1–481.

Cranford, T. W., Krysl, P., and Amundin, M. (2010). "A new acoustic portal into the odontocete ear and vibrational analysis of the tympanoperiotic complex," *PLoS ONE* **5**(8), e11927.

Currey, J. D. (1978). "Mechanical properties of bone tissues with greatly differing functions," *J. Biomech.* **12**, 313–319.

Dallos, P. (1970). "Low-frequency auditory characteristics: Species dependence," *J. Acoust. Soc. Am.* **48**, 489–499.

Elkhouiri, N., Liu, H., and Funnell, W. R. J. (2006). "Low-frequency finite-element modeling of the gerbil middle ear," *J. Assoc. Res. Otolaryngol.* **7**, 399–411.

Fleischer, G. (1978). "Evolutionary principles of the mammalian middle ear," *Adv. Anat., Embryol. Cell Biol.* **55**(5), 3–70.

Fraser, F. C., and Purves, P. E. (1954). "Hearing in cetaceans," *Bull. Brit. Mus.* **2**(5), 103–116.

Gan, R. Z., Feng, B., and Sun, Q. (2004). "Three-dimensional finite element modeling of human ear for sound transmission," *Ann. Biomed. Eng.* **32**(6), 847–859.

Gedamke, J., Costa, D. P., and Dunstan, A. (2001). "Localization and visual verification of a complex minke whale vocalization," *J. Acoust. Soc. Am.* **109**(6), 3038–3047.

Guinan, J. J., Jr., and Peake, W. T. (1967). "Middle-ear characteristics of anesthetized cats," *J. Acoust. Soc. Am.* **41**(5), 1237–1261.

Heffner, R. S., and Heffner, H. E. (1985). "Hearing range of the domestic cat," *Hear. Res.* **19**(1), 85–88.

Heffner, R. S., and Heffner, H. E. (1991). "Behavioral hearing range of the chinchilla," *Hear. Res.* **52**(1), 13–16.

Homma, K., Du, Y., Shimizu, Y., and Puria, S. (2009). "Ossicular resonance modes of the human middle ear for bone and air conduction," *J. Acoust. Soc. Am.* **125**(2), 968–979.

ISO (1996). 389-7, *Acoustics: Reference zero for the calibration of audiometric equipment. Part 7: Reference threshold of hearing under free-field and diffuse-field listening conditions* (International Organization for Standardization, Geneva, Switzerland).

Johnson, C. S. (1968). "Sound detection thresholds in marine mammals," in *Marine Bioacoustics*, edited by W. N. Tavolga (Pergamon, New York), Vol. 2, pp. 247–260.

Johnson, C. S., McManus, M. W., and Skaar, D. (1989). "Masked tonal hearing thresholds in the beluga whale," *J. Acoust. Soc. Am.* **85**(6), 2651–2654.

Ketten, D. R. (1994). "Functional analyses of whale ears: Adaptations for underwater hearing," *IEEE Proc. Underwater Acoustics* **1**, 264–270.

Ketten, D. R. (2000). "Cetacean ears," in *Hearing by Whales and Dolphins*, edited by W. W. L. Au, A. N. Popper, and R. R. Fay (Springer, New York), pp. 43–108.

Ketten, D. R. (2002). "Marine mammal auditory systems: A summary of audiometric and anatomical data and implications for underwater acoustics impacts," *Polarforschung* **72**, 79–92.

Kibblewhite, A. C., and Jones, D. A. (1976). "Ambient noise under Antarctic sea ice," *J. Acoust. Soc. Am.* **59**(4), 790–798.

Koike, T., Wada, H., and Kobayashi, T. (2002). "Modeling of the human middle ear using the finite-element method," *J. Acoust. Soc. Am.* **111**(3), 1306–1317.

Ladak, H. M., and Funnell, W. R. J. (1996). "Finite-element modeling of the normal and surgically repaired cat middle ear," *J. Acoust. Soc. Am.* **100**(2), 933–944.

Lay, D. M. (1972). "The anatomical, physiological, functional significance, and evolution of specialized hearing organs of gerbilline rodents," *J. Morphol.* **138**, 41–120.

Miller, B. S., Zosuls, A. L., Ketten, D. R., and Mountain, D. C. (2006). "Middle-ear stiffness of the bottlenose dolphin *Tursiops truncatus*," *IEEE J. Ocean. Eng.* **31**(1), 87–94.

Norris, K. S. (1964). "Some problems of echolocation in cetaceans," in *Marine Bioacoustics*, edited by W. N. Tavolga (Pergamon, New York), pp. 317–336.

Nowacek, D. P., Thorne, L. H., Johnston, D. W., and Tyack, P. L. (2007). "Responses of cetaceans to anthropogenic noise," *Mammal Rev.* **37**(2), 81–115.

Nummela, S., Wägar, T., Hemilä, S., and Reuter, T. (1999). "Scaling of the cetacean middle ear," *Hear. Res.* **133**, 71–81.

Oliver, W. C., and Pharr, G. M. (1992). "An improved technique for determining hardness and elastic modulus using load and displacement sensing indentation experiments," *J. Mater. Res.* **7**, 1564–1583.

Prendergast, P. J., Ferris, P., Rice, H. J., and Blayney, A. W. (1999). "Vibro-acoustic modeling of the outer and middle ear using the finite-element method," *Audiol. Neuro-Otol.* **4**(3-4), 185–191.

Puria, S. (2003). "Measurements of human middle ear forward and reverse acoustics: Implications for otoacoustic emissions," *J. Acoust. Soc. Am.* **113**(5), 2773–2789.

Purves, P. E. (1955). "The wax plug in the external auditory meatus of the Mysticeti," *Discovery Reports* **27**, 293–302.

Rho, J.-Y., Tsui, T. Y., and Pharr, G. M. (1997). "Elastic properties of human cortical and trabecular lamellar bone measured by nano-indentation," *Biomaterials* **18**(20), 1325–1330.

Rosowski, J. J. (1991). "The effects of external- and middle-ear filtering on auditory threshold and noise-induced hearing loss," *J. Acoust. Soc. Am.* **90**(1), 124–135.

Rosowski, J. J. (1994). "Outer and middle ears," in *Comparative Hearing: Mammals*, edited by R. R. Fay and A. N. Popper (Springer, New York), pp. 172–247.

Ruggero, M. A., Rich, N. C., Robles, L., and Shivapuja, B. G. (1990). "Middle-ear response in the chinchilla and its relationship to mechanics at the base of the cochlea," *J. Acoust. Soc. Am.* **87**(4), 1612–1629.

Ruggero, M. A., and Temchin, A. N. (2002). "The roles of the external, middle, and inner ears in determining the bandwidth of hearing," *Proc. Natl. Acad. Sci. U.S.A.* **99**, 13206–13210.

Ryan, A. (1976). "Hearing sensitivity of the Mongolian gerbil, *Meriones unguiculatus*," *J. Acoust. Soc. Am.* **59**(5), 1222–1226.

Szymanski, M. D., Bain, D. E., Kiehl, K., Pennington, S., Wong, S., and Henry, K. R. (1999). "Killer whale (*Orcinus orca*) hearing: Auditory brainstem response and behavioral audiograms," *J. Acoust. Soc. Am.* **106**(2), 1134–1141.

- Urick, R. J. (1983). *Principles of Underwater Sound* (McGraw-Hill, New York), pp. 1–423.
- von Békésy, G. (1960). *Experiments in Hearing*, translated and edited by E. G. Wever (McGraw-Hill, New York), pp. 1–745.
- Wada, H., Metoki, T., and Kobayashi, T. (1990). “Analysis of dynamic behavior of human middle ear using a finite-element method,” *J. Acoust. Soc. Am.* **92**(6), 3157–3168.
- Wartzok, D., and Ketten, D. R. (1999). “Marine mammal sensory systems,” in *Biology of Marine Mammals*, edited by J. Reynolds and S. Rommel (Smithsonian Institution, Washington, DC), pp. 117–175.
- Wever, E. G., and Lawrence, M. (1954). *Physiological Acoustics* (Princeton University Press, Princeton, NJ), pp. 1–454.
- Willi, U. B., Ferrazzini, M. A., and Huber, A. M. (2002). “The incudo-malleolar joint and sound transmission losses,” *Hear. Res.* **174**(1/2), 32–44.
- Yamato, M., Ketten, D. R., Arruda, J., Cramer, S., and Moore, K. (2012). “The auditory anatomy of the minke whale (*Balaenoptera acutorostrata*): A potential fatty sound reception pathway in a baleen whale,” *Anat. Rec.* **295**, 991–998.
- Zioupos, P. (2005). “*In vivo* fatigue microcracks in human bone: Material properties of the surrounding bone matrix,” *Eur. J. Morphol.* **42**(1/2), 31–41.